Engine Emission Modeling Using a Mixed Physics and Regression Approach

Michael Benz
e-mail: mbenz@alumni.ethz.ch

Christopher H. Onder

Lino Guzzella

Department of Mechanical and Process Engineering,
ETH Zurich,
8092 Zurich, Switzerland

This paper presents a novel control-oriented model of the raw emissions of diesel engines. An extended quasistationary approach is developed where some engine process variables, such as combustion or cylinder charge characteristics, are used as inputs. These inputs are chosen by a selection algorithm that is based on genetic-programming techniques. Based on the selected inputs, a hybrid symbolic regression algorithm generates the adequate nonlinear structure of the emission model. With this approach, the model identification efforts can be reduced significantly. Although this symbolic regression model requires fewer than eight parameters to be identified, it provides results comparable to those obtained with artificial neural networks. The symbolic regression model is capable of predicting the behavior of the engine in operating points not used for the model parametrization, and it can be adapted easily to other engine classes. Results from experiments under steady-state and transient operating conditions are used to show the accuracy of the presented model. Possible applications of this model are the optimization of the engine system operation strategy and the derivation of virtual sensor designs. [DOI: 10.1115/1.3204510]

1 Introduction

Diesel engines are often used for heavy-duty (HD) as well as passenger car applications due to their lower fuel consumption compared with gasoline engines. One disadvantage of diesel engines is the fact that they emit relatively high amounts of nitrogen oxides (NO_x) and particulate matter (PM). Due to the more stringent future emission legislation, exhaust aftertreatment devices and sophisticated operation strategies for the entire engine system are necessary.

In contrast to gasoline engines, where the aftertreatment problem is solved by using an efficient three-way catalyst, there is no aftertreatment system for diesel engines established as yet. The reduction of PM is often tackled by using a diesel particle filter (DPF), with the disadvantages of a higher fuel consumption due to the higher backpressure in the exhaust system and the necessary regeneration of the particle filter. A NO_x trap with an impact on the fuel consumption or a selective catalytic reduction (SCR) catalyst are typically used to reduce emissions of nitrogen oxides. The engine control system cannot be optimized separately from the operation strategy of the aftertreatment devices due to the strong interactions between them. Furthermore, the optimal operation of a diesel engine itself is a highly complex task. Several actuators affect the gas path and the diesel injection system. Figure 1 shows the gas path of a modern diesel engine and its components and actuators. On the basis of limited test bench availability due to economic and time restrictions, mathematical models are an essential tool for optimizing the configuration and the operation strategies in static as well as in transient operation modes. This target can be reached only with fast yet accurate models based on a physics-oriented approach to guarantee their fast application to other engines.

In this research, various techniques are used to derive a mathematical model of the raw emissions. The nonlinear extended quasistatic emission and combustion model is derived by a symbolic regression (SR) algorithm. The inputs to the SR algorithm are characteristic engine process variables such as combustion center and air mass in the cylinder. These variables are chosen by an input variable selection (IVS) algorithm. The IVS algorithm is based on genetic-programming (GP) and artificial neural network (ANN) techniques. The enveloping gas path structure is represented by a mean-value engine model. The raw emission model (REM) is validated with two measurement data sets of a heavy-duty and a light-duty (LD) diesel engine.

2 Current Modeling Approaches

To model the gas path of the engine, mean-value models are the state of the art for control-oriented applications (see, for example, Refs. [1,2]). The mean-value model approach shows a good compromise between computational efficiency and accuracy. The relevant engine dynamics are represented by ordinary differential equations. The combustion is then often treated as quasistatic in this modeling approach since the gas path actuators used cannot influence or control the fast dynamics of the combustion process. At any given engine speed, the torque produced is highly correlated with the actual fuel mass flow, even in transient operating conditions. In contrast, the engine raw emissions can vary strongly during transient operation of the engine because the boundary conditions of the combustion process, such as boost pressure or exhaust gas recirculation (EGR) rate, influence the emission formation significantly [3].

For the engine raw emissions, a control-oriented modeling approach is not established as yet. Current models reported in literature can be divided into three main categories:

- empirical models [4,5]
- phenomenological models [6]
- three-dimensional computational fluid dynamics (CFD) models [7]

The phenomenological and the CFD models are usually crank angle based and describe the in-cylinder processes in detail. Because of the high computational costs of these models, such approaches are not feasible for transient simulations that must run much faster than real time. Event- or time-based empirical models are computationally more efficient. Therefore, they can be used for real-time simulations. Black-box models are typical examples of this class of models. Since the internal structure of the system is unknown, the input/output behavior is modeled with either an

Manuscript received March 10, 2009; final manuscript received June 4, 2009; published online January 19, 2010. Review conducted by Christopher J. Rutland.

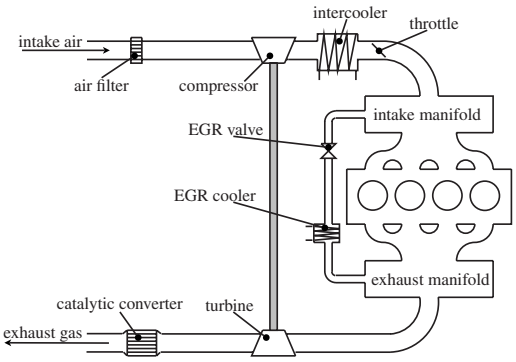

Fig. 1 Illustration of a standard diesel engine gas path and its components

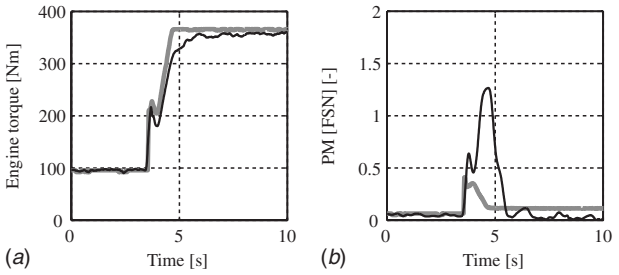

Fig. 2 Comparison between measurement data (black) and results of quasistationary simulations (gray) during a load step at constant engine speed: (*a*) engine torque and (*b*) PM

ANN algorithm or with a polynomial approach (see, for example, Refs. [4,5]). The disadvantage of such a black-box modeling approach is the vast number of measurements needed to identify the parameters. This large number of parameters limits the portability of such models to other engine types or even to other operating points. An approach used to overcome these limitations is the use of a phenomenological model to produce simulation data to calibrate the black-box models. This is a very promising approach for future investigation, but the accuracy of the phenomenological models to substitute measurement data is not sufficient yet.

Another approach is the use of so-called gray-box models, which reflect some of the internal physical laws. A simple polynomial approach is presented in Ref. [8], where a statistical model of the (NO_x) emissions was developed. That model is based on relevant process variables. Because of the rather physics-based inputs, the model is suitable to being applied on different engine types. A quasistatic approach is presented in Ref. [3]. The transient emissions are calculated by static base maps with transient correction factors, which are functions of the actual air/fuel ratio. An ANN approach is presented in Ref. [9] based on characteristic pressure trace variables such as combustion center, maximum heat release rate, or peak pressure generated from steady-state measurements. The ANN is validated on measurement data from a transient driving cycle. del Re and Langthaler [10] presented a model based on a SR algorithm to estimate the nitrogen oxide emissions directly from the electronic control unit (ECU) signals. The dynamics of the gas path and the sensors are included in the equation derived.

3 Quasistationary Simulations

Quasistationary simulations (QSSs) assume that maps are available that describe the correlation between the current operating point of the engine defined by engine speed and fuel mass flow and the outputs such as torque production. In this research, the pollutant emission outputs that are subjected to legal limits are stored in such base maps as well. These maps are built with stationary measurement data of the entire operation range of the engine. The inputs into these maps are engine speed and fuel mass flow, which represent the actual operating point. The operating point variables are scaled in order to increase the portability of the models generated. The engine speed is expressed as the mean piston speed

$$c_m = \frac{\omega_e S}{\pi} \tag{1}$$

where ω_e is the engine speed and S is the stroke. The injected fuel mass flow $\dot{m}_i$ is scaled by the engine speed, the displacement value V_d, and the lower heating value H_l of the fuel. The fuel mean pressure is then calculated as

$$p_{\mathrm{mf}} = \frac{H_l \dot{m}_i 4\pi}{V_d \omega_e} \tag{2}$$

Using these maps, QSSs can be performed. For instance, the quasistationary value of the engine torque is calculated as

$$T_{\mathrm{eng0}} = f(c_m, p_{\mathrm{mf}}) \tag{3}$$

The quasistationary values stored in the base map are linearly interpolated for the current operating point defined by mean piston speed and fuel mean pressure. Quasistationary simulations are useful for calculating the fuel consumption on a transient cycle. The quasistatic assumption fails for the calculation of engine-out emissions, as already mentioned in the previous section. Figure 2 shows a comparison between measurement data and results of quasistationary simulations of the engine torque and the PM emissions during a load step. Clearly, the data of the engine torque and the quasistationary simulation agree quite well. In contrast, the PM emissions of the engine are substantially different from the model prediction. During the transient phase, the amount of PM emissions detected is significantly higher than the quasistationary values. These deviations can be explained by analyzing the boundary condition of the combustion process.

Figure 3 shows the difference between measurement data and results of quasistationary simulations of the gas path variables and injection actuators during a load step at constant engine speed. The relevant gas path variables are boost pressure, EGR rate, and the temperature after the intercooler. These variables influence the mass and the gas composition in the cylinder when the intake valve is closed. The injection actuators are start of injection, fuel rail pressure, and injection duration. The turbocharger inertia causes the most significant dynamic effect in a modern direct injection (DI) diesel engine in that it influences significantly the boost pressure and the EGR rate during transient operation. The so-called turbo lag is responsible for the high PM emission during load steps or in fast acceleration phases (low gear) because these slow dynamics yield a relatively low air/fuel ratio of the cylinder charge. Due to the simultaneous occurrence of an EGR rate peak, the PM emissions are further increased. The start of injection follows mostly the quasistationary value in transient operating conditions. During a tip-in, the common-rail injection system cannot follow the desired fuel rail pressure. This leads to longer injection times, which increases the PM emissions during a few engine cycles. The longer injection time causes the first PM emission peak during the load step shown in Fig. 2. The influence on the transient engine raw emission of the cylinder wall temperature is negligibly small [11]. Therefore, the temperature effects are neglected in the further investigations. The relevant boundary conditions of the combustion and emission formation can be summarized as

- operating point (injected fuel and engine speed)
- cylinder charge (mass, gas composition, and gas temperature in the cylinder when the intake valve is closed)

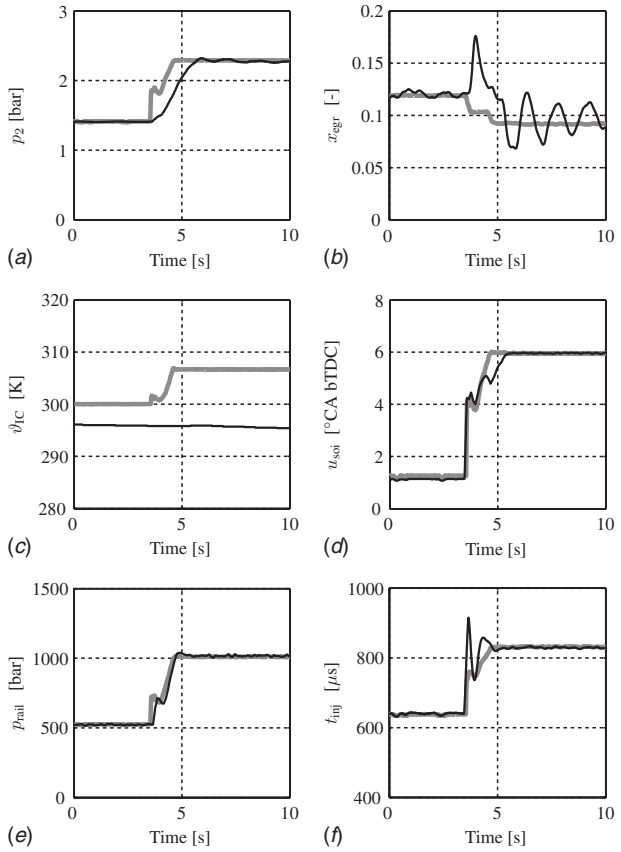

Fig. 3 Comparison between measurement data (black) and results of quasistationary simulations (gray) during a load step at constant engine speed: (*a*) boost pressure, (*b*) EGR rate, (*c*) temperature after intercooler, (*d*) start of main injection, (*e*) fuel rail pressure, and (*f*) injection duration

- injection (fuel rail pressure, start, duration, and split of injection events)

The deviations of the boundary conditions are considered in the extended quasistationary REM using correction factors. The extension describes the static and transient deviations of the raw emissions compared with the quasistationary values. An overview of the control-oriented REM is presented in the next section.

4 Overview of the Control-Oriented Model

The basic structure of the proposed control-oriented modeling approach is shown in Fig. 4 for the NO_x emissions. The proposed

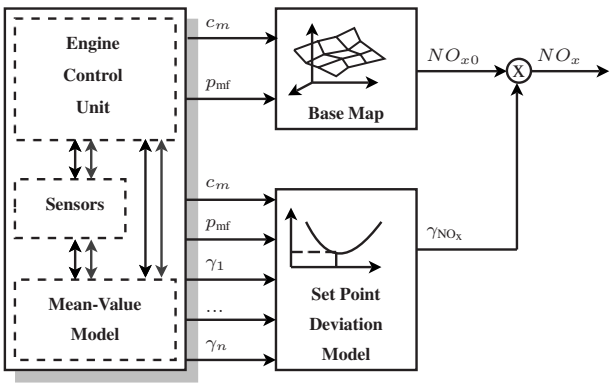

Fig. 4 Control-oriented NO_x emission model formulation

nonlinear nitrogen oxide model consists of two static parts. In the base map part,

$$NO_{x0} = f(c_m, p_{mf}) \tag{4}$$

the quasistationary output value NO_{x0} is a function of the actual mean piston speed c_m and the fuel mean pressure p_{mf}. The second part is the nonlinear set point deviation model. This extension models the transient deviations or static offsets of the NO_x emission values due to the changed boundary conditions of the combustion. The output of the set point deviation model is the correction factor γ_{NO_x}. This correction factor models the ratio between the actual NO_x emissions and the NO_x base map value. The NO_x correction factor is modeled as a function of the operating point variable mean piston speed and fuel mean pressure as well as the additional inputs γ_i. Since the influences of these additional inputs may vary in the operating range, the operating point variables have to be included in the correction factor γ_{NO_x} model,

$$\gamma_{NO_x} = f(c_m, p_{mf}, \gamma_1, \gamma_2, \ldots, \gamma_n) \tag{5}$$

The inputs γ_i are the ratios of relevant engine process variables to their base map values. These variables represent the relevant boundary condition of the combustion. An input variable selection algorithm selects these variables. The selection algorithm and the relevant engine process variables used are discussed in detail in Sec. 5. The variables γ_i are calculated as

$$\gamma_i = \frac{u_i}{u_{i0}} \tag{6}$$

where u_i is the actual value of the relevant engine process variable. The base map value u_{i0} of this relevant engine process variable again depends on the actual mean piston speed and the fuel mean pressure,

$$u_{i0} = f(c_m, p_{mf}) \tag{7}$$

The actual emissions value NO_x is then calculated as a multiplication of the base map value and the NO_x correction factor,

$$NO_x = \gamma_{NO_x} NO_{x0} \tag{8}$$

Neither the correction factor nor the base map value has any additional dynamics. The dynamics are considered only in the transient behavior of the inputs γ_i. The structure is similar to that of the approach reported in Ref. [12], where the proposed linear set point deviation model is adopted as a virtual sensor to estimate and control the actual NO_x emissions at the engine out. Compared with Ref. [12], the main difference in this research is the nonlinear formulation of the set point deviation model. Since the PM emissions act highly nonlinear to air/fuel-ratio deviations, the linear assumption would not be appropriate. Additionally, since the model should cover the entire operating range of the engine, large deviations from the standard operating point settings can occur in all boundary conditions. The model can be calibrated with static measurement data due to the quasistationary formulation. This simplifies the parametrization significantly.

The relevant engine process variables used as inputs into the set point deviation model can be provided by a mean-value model or by sensor signals. The application area of the REM defines the final enveloping structure (see Sec. 6). The derivation of the set point deviation model is presented in more detail in the next section.

5 Set Point Deviation Model

An important starting point for the design of the set point deviation model is the choice of the relevant inputs. Therefore, the inputs are selected by an IVS algorithm [13]. Possible inputs are characteristic engine process variables such as combustion center or cylinder mass. The efficient structure of the model is prepared by a symbolic regression algorithm based on genetic-programming techniques [14]. While the symbolic regression

could also be used as an IVS algorithm, the advantage of separating the two steps is a reduced calculation time. The derivation of the model (ANN) used in the IVS algorithm takes around 10 s on a modern desktop computer. In contrast, for a given input combination on the same computer, the symbolic regression needs more than 50 h to find the expected structure. A good selection of inputs with a poorly trained symbolic regression still has an insufficient fitness value. Therefore, it is likely not chosen for the next generation. In addition, the separation simplifies the application of specifications to the number of inputs. Clearly, using the symbolic regression as an IVS algorithm is thus not recommended.

The advantage of these process-relevant inputs and their functional coherence to the emission values is the reduction of parameters needed to describe the emission formation. The adequate and therefore efficient structure reduces calculation time. The design procedure of the set point deviation model can be divided into three main steps:

1. definition of the relevant process variables by expert knowledge
2. selection of candidate variables from a set of characteristic process variables using the IVS algorithm
3. determination of a lean model structure based on the SR algorithm

The three steps are discussed in detail in Secs. 5.1–5.3.

5.1 Characteristic Process Variables of the Engine. Most of the inputs (actuator values) into the system do not influence the emission values directly. The following line of action exemplifies; the EGR valve actuator signal implies an open valve area. This valve area yields a certain EGR mass flow, which influences the cylinder charge when the intake valve is closed. Finally, the exhaust gas mass in the cylinder significantly influences the raw emissions. Therefore, the model complexity can be reduced using directly the exhaust gas mass in the cylinder instead of using the actuator signal as an input.

Analogously to this example, typical engine process variables must be defined first. The number of process variables used as inputs should be equal to or less than the number of actuators of the system. Otherwise, an overdetermined system results. Table 1 shows the characteristic process variables used. Of course, the list is not complete, and other variables could be added. In addition, the actuator input signals are added. The values that are not measured directly are estimated. The EGR fraction in the intake manifold is estimated based on the CO_2 measurement signal in the intake and exhaust receivers. The cylinder charge is estimated based on the EGR ratio and the intake mass flow sensor signal.

The total cylinder charge is thus composed of intake air, external EGR, internal EGR, and injected fuel mass. The cylinder charge is divided into an air fraction (x_{air}) and an exhaust gas fraction (x_{eg}) with a stoichiometric air/fuel ratio. A one-zone heat release analysis is performed to obtain the in-cylinder process variables. The model used to calculate the liquid fuel length and the lift-off length of the injection spray is proposed by Refs. [15,16]. The next step is to find the best combination of these process variables to build the inputs into the correction factor model. It is not possible to calculate all combinations of inputs due to the limited computational resources [17]. Therefore, an input selection algorithm based on GP techniques is used to choose a promising combination out of the potential inputs. In total, 40 potential inputs are delivered to the IVS algorithm. The transient estimation of the used relevant engine process variables is discussed in Sec. 6.

5.2 Input Variable Selection Algorithms. The IVS is the next step in the modeling approach. If the system is well known, the relevant inputs into the system can be selected by expert knowledge. Often, the coherences of physical systems are not well understood or they are computationally expensive to model. The practitioner thus needs an algorithm that selects the relevant inputs directly from measurement data. Algorithms for the IVS task can be classified in wrapper (model-based) or filter (model-free) methods (for details, see Refs. [18,13]). Both approaches are briefly discussed next. Filter techniques utilize a statistical measure to decide the interdependencies of the input and output variables as the basis for the IVS. A popular method for the input selection is the principal component analysis (PCA) [19]. Its drawback is its sensitivity to noise and data transformations. The underlying assumption of a linear structure is contradictory to the present highly nonlinear system being analyzed here. For a nonlinear system, a common procedure for a filter-based IVS approach has not been established yet in the scientific community.

In contrast, the wrapper approach used in this study treats the input selection search as an optimization of an arbitrary model structure. The input selector exists as a wrapper around the fitness evaluation and the model calibration block. Figure 5 shows the procedure of the wrapper approach. The input selection search

Table 1 The 40 characteristic process variables used

Actuator signals	
u_{vtg}	Variable turbine geometry input
u_{egr}	EGR valve input
u_{soi}	Start of injection
p_{rail}	Actual fuel rail pressure
t_{inj}	Injection duration
u_{thr}	Throttle input
Gas path variables	
p_{im}	Intake manifold pressure
ϑ_{im}	Intake manifold temperature
$\dot{m}_{\mathrm{egr}}$	EGR mass flow
$\dot{m}_{\mathrm{ia}}$	Intake air mass flow
p_{em}	Exhaust manifold pressure
ϑ_{em}	Exhaust manifold temperature
$\dot{m}_{\mathrm{turb}}$	Turbine mass flow
λ	Air/fuel ratio
n_{turb}	Turbocharger speed
Cylinder charge	
m_e	Total mass
m_{air}	Air mass
$m_{\mathrm{O_2}}$	Oxygen mass
$m_{\mathrm{CO_2}}$	Carbon dioxide mass
m_{eg}	Exhaust gas mass
x_{air}	Air ratio
$x_{\mathrm{O_2}}$	Oxygen ratio
$x_{\mathrm{CO_2}}$	Carbon dioxide ratio
x_{eg}	Exhaust gas ratio
Combustion characteristics	
τ_{ID}	Ignition delay
φ_{B01}	Start of combustion
φ_{B05}	Location of 5% fuel mass burnt
φ_{B10}	Location of 10% fuel mass burnt
φ_{B50}	Location of 50% fuel mass burnt
φ_{B90}	Location of 90% fuel mass burnt
φ_{B95}	End of combustion
$\Delta\varphi_{B10-B50}$	Duration from φ_{B10} to φ_{B50}
$\Delta\varphi_{B50-B90}$	Duration from (φ_{B50} to φ_{B90})
$\Delta\varphi_{\mathrm{comb}}$	Combustion duration ($\varphi_{B01}-\varphi_{B95}$)
p_{max}	Peak cylinder pressure value
$\varphi_{p_{\mathrm{max}}}$	Location of peak cylinder pressure
$\dot{q}_{\mathrm{max}}$	Maximum heat release rate (HRR)
$\varphi_{\dot{q}_{\mathrm{max}}}$	Location of maximum HRR
Injection spray	
l_l	Liquid spray length
l_{lo}	Lift-off length
λ_{comb}	Air/fuel ratio of initial combustion

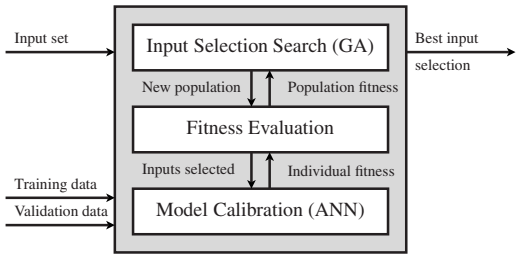

Fig. 5 The wrapper approach as an input selection algorithm

proposes a potential subset of all the possible inputs. The fitness evaluator calculates a fitness value for each subset to estimate the performance of the selection. Therefore, the chosen model structure is calibrated using the selected inputs. Once a certain performance is reached, the algorithm finishes. A frequently used input selection search is the forward or backward selection, where the number of inputs is systematically increased or decreased by the most or least relevant inputs, respectively. Its drawback is that it yields only a suboptimal subset selection, especially if the initial set of possible inputs includes highly correlated variables. Heuristic techniques based on trial and error or so-called brute-force approaches can be used to find the optimal subset. These selection algorithms require an exhaustive search. If large numbers of possible inputs are available, these approaches are computationally expensive. Thousands of input combinations require a calibration of the model structure. Hence, for practical algorithms, the search is conducted for a satisfactory subset instead of an optimal subset.

An algorithm based on genetic-programming techniques is used in this study to find a promising subset [14]. Each individual of the population is represented by a bit string where 1 means that the input is selected and 0 means that the input is not selected. After estimating the performance of each individual, a new population is generated. Figure 6 shows the scheme used to produce the new generation of individuals. The parameters of the IVS algorithm used are shown in Table 2. The best individuals proceed directly to the new generation (elitism). The others are stochastically chosen for reproduction. Crossover and point mutation are used as genetic operators. Due to the fact that only a small subset of potential inputs is to be selected, the mutation rate from 1 to 0 is higher than that from 0 to 1. The unequal mutation rate enhances individuals with nearly the desired number of inputs. Therefore, the algorithm converges faster. The fitness value of the actual individuals is tested by a model. The model to estimate the output values can be a polynomial (see Ref. [20]). Because of its higher flexibility, the output is calculated with a feedforward ANN in this study. The ANN is adapted to the training data points y for every new combination of inputs in the actual population. The fitness value and model output $\hat{y}$ of each combination is then stored in memory to avoid multiple evaluations of the same selection. The fitness value of the selection is calculated as the mean

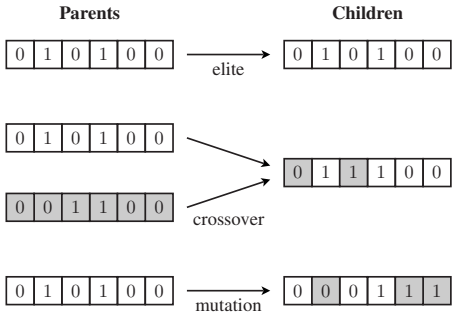

Fig. 6 Bit string manipulation of the input selection algorithm

Table 2 Parameters of the input selection algorithm

Population size	500
Generations	≈100
Desired number of inputs	3
Elitism fraction	0.1
Genetic operators	Mutation, crossover
Crossover function	Stochastic uniform
Crossover fraction	0.25
Mutation function	Uniform
Mutation fraction	0.65
Mutation rate to 1	0.075
Mutation rate to 0	0.925
Selection function	Stochastic uniform

square error and is additionally penalized with the factor f if the number of the selected inputs n_{sel} exceeds the desired quantity n_{des}. The input selection search minimizes this fitness value J,

$$J = \frac{1}{m}\sum_{k=1}^{m} (y(k) - \hat{y}(k))^2 f \tag{9}$$

where m is the number of measurement data and f is

$$f = \begin{cases} 1 & \text{if } n_{sel} \leq n_{des} \\ n_{sel} - n_{des} + 1 & \text{if } n_{sel} > n_{des} \end{cases} \tag{10}$$

The stopping criterion is reached after the stagnation of the fitness value during 20 generations. The desired quantity of inputs is set to 3, in addition to the operating point variables (mean piston speed and fuel mean pressure). The ANN used has four neurons in two hidden layers with four neurons and a linear output layer. The transfer functions used are hyperbolic tangent sigmoid functions. The number of parameters depends on the number of inputs. If five inputs are selected, the number of parameters is 49 for the ANN structure used. Hence, a large number of measurement data points are necessary to calibrate the ANN. The measurement data set is divided into a training data and a validation data set. The best fitness value of the population stagnates approximately after 100 generations. If the population size is 500, 50,000 neural networks need to be adapted to the data set.

The result of the IVS algorithm is the Pareto front with the best combination of inputs found. The Pareto front gives reliable results between one and approximately eight additional inputs. Figure 7 clearly shows that the fitness value of the NO_x emissions decreases significantly until three additional inputs to the operating point variables are reached. The benefit of a higher complexity is very low. The six actuators ($u_{egr}, u_{thr}, u_{vtg}, u_{soi}, u_{p_{rail}}, t_{inj}$) and the engine speed can be summarized into three relevant process variables and the two operating point variables. If more than six or

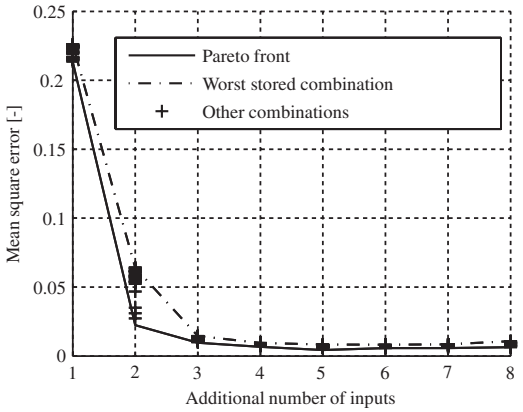

Fig. 7 Pareto front of the input selection algorithm for the normalized nitrogen oxide emissions without factor *f*

seven inputs into the model are used, the fitness value gets even worse. The calibration algorithm of the ANN finds only a suboptimal solution for the large number of parameters in this case. There are two likely explanations for this effect. Either the problem is overparametrized or the input range is overdetermined; i.e., several inputs or combinations of them contain equivalent informations. Both cases result in an overfitted ANN, which performs worse on the validation data. Additionally, fewer possible combinations are tested with more than eight parameters due to the extra penalty of the fitness value.

As expected, multiple combinations of inputs (due to the redundant information) yield nearly the same fitness value in the case of three or more inputs. If only two inputs are selected, the choice of the input subset is more sensitive. Thus, the engineer can choose a combination of "cheap" inputs. Inputs are called cheap if they are variables directly measured by a standard sensor or they can be easily calculated based on available sensor signals.

The authors recommend the following input combination for the nitrogen oxides:

- operating point (mean piston speed, fuel mean pressure)
- cylinder mass when the intake valve is closed m_e
- air fraction in the cylinder when the intake valve is closed x_{air}
- combustion center φ_{B50}

which results in the following equation for the NO_x correction factor

$$\gamma_{NO_x} = f(c_m, p_{\text{mf}}, \gamma_{m_e}, \gamma_{x_{\text{air}}}, \gamma_{\varphi_{B50}}) \tag{11}$$

Then, inserting Eq. (11) into Eq. (8) yields the actual NO_x emission value. The following inputs are recommended for the PM emissions:

- operating point (mean piston speed and fuel mean pressure)
- cylinder air mass when the intake valve is closed m_{air}
- fuel rail pressure p_{rail}
- location of the 90% fuel mass burnt φ_{B90}

The PM correction factor is then estimated as

$$\gamma_{\text{PM}} = f(c_m, p_{\text{mf}}, \gamma_{m_{\text{air}}}, \gamma_{p_{\text{rail}}}, \gamma_{\varphi_{B90}}) \tag{12}$$

In the next step, the parameter-intensive ANN is replaced with a lean model structure determined by the SR algorithm.

5.3 Structure Derivation Based on Symbolic Regression. As mentioned in the introduction of this section, the structure of the set point deviation model is found with a SR algorithm [14]. For all the SR calculations, the GPLab toolbox for MATLAB® is used [21]. The toolbox is equipped with state-of-the-art genetic operators, survival, and reproduction methods. The individuals of the population are stored in a tree. Figure 8 shows the tree structure and the possible tree manipulations. Two kinds of mutation can occur. The first is the point mutation where several nodes are mutated independently. Second is the tree mutation where a part of the tree is exchanged with a new randomly generated tree. The new tree part has a maximal size of six nodes (initial maximal level). Due to the open source code, the toolbox can easily be extended with the user's own methods. GPLab uses functions and terminals to represent the individuals. Any mathematical operation can be used as a function. In this investigation, the functions addition, multiplication, division, exponential, and the power function are used.

Terminals can be input variables $(u_1, \ldots, u_n)$, parameters $(c_1, \ldots, c_8)$, constants (e.g., π), or random numbers. The parameters are optimized by a local search algorithm for every individual separately. The toolbox is therefore extended with a local search algorithm based on a Nelder-Simplex approach [22]. The maximum number of variable parameters is approximately 8.

The symbolic regression is performed for two different engine

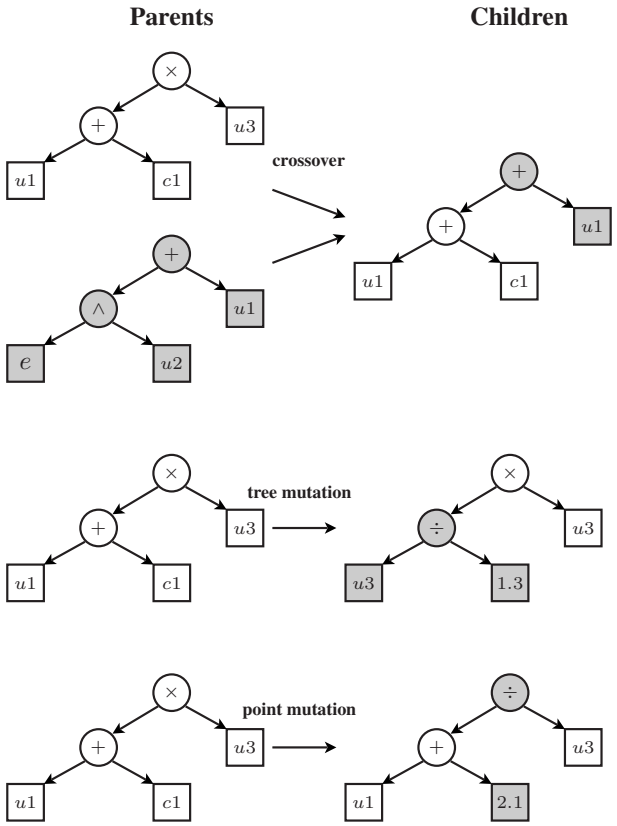

Fig. 8 Symbolic regression: tree manipulations

emission data sets in parallel. The data sets of both engines include approximately 300 static measurement points. Each data set contains a base map of the engine and additionally measurement data points, where all the actuator inputs are varied in six relevant operating points, well distributed over the engine operating range. The inputs and the resulting tree structure used are the same for both data sets. Only the variable parameters are calibrated by the local search algorithm for both data sets separately. The fitness value of each individual is then calculated as the sum of the mean square errors of both data sets.

The data sets used to generate and to calibrate the REM are discussed in Sec. 7. Figure 9 compares the NO_x emission fitness values for various maximal tree size limits. The fitness values decrease significantly up to a limit of 15 nodes for both data sets. If the limit is set higher than 40 nodes, the mean square error marginally decreases. Therefore, the maximal number of nodes is set between 25 and 40. Oversized individuals are filtered out and replaced by randomly generated new trees. All the important settings of the symbolic regression algorithm used are shown in

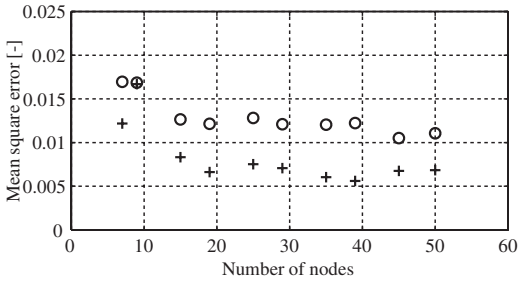

Fig. 9 Fitness value for the NO_x emissions for the two different data sets: light-duty engine (circle) and heavy-duty engine (cross)

Table 3 Parameters of the symbolic regression algorithm

Population size	1000
Generations	≈100
Functions	Plus, times, power, divide, exponential
Terminals	Constant, random number, parameter
Number of parameters	8
Genetic operators	Crossover, mutation
Mutation	Point/tree
Maximal tree size	25–40 nodes
Initial maximal level	6
Elitism	Keep best

Table 3.

The resulting function for the NO_x correction factor γ_{NO_x} is

$$(\gamma_{\varphi_{B50}} \cdot \gamma_{x_{air}}^{\gamma_{x_{air}}+C_5})^{C_8 \cdot a \cdot b} \tag{13}$$

where a and b are defined as

$$a = \left(\frac{\gamma_{\varphi_{B50}}}{\gamma_{x_{air}}} \right)^{C_4 \cdot \gamma_{m_e}+C_2} \tag{14}$$

$$b = \frac{\gamma_{\varphi_{B50}}}{c_m} + C_7 \tag{15}$$

The mean fuel pressure is not included in the function. Hence, the influence of the load on the correction factor is negligible. Furthermore, not all of the variable parameters are used. The resulting formula has five variable parameters.

The generated function for the PM correction factor γ_{PM} is

$$\gamma_{PM} = (\gamma_{m_{air}}^{a^{\gamma_{m_{air}}}(C_1/\gamma_{\varphi_{B90}})^{-\gamma_{p_{rail}}}})^{C_4 \cdot b} \tag{16}$$

where a and b are defined as

$$a = \frac{C_2 \gamma_{m_{air}}^{C_3}}{\gamma_{p_{rail}}} + C_6 \tag{17}$$

$$b = p_{mf} + \gamma_{\varphi_{B90}} + C_7 \tag{18}$$

The mean piston speed is not selected as an input. The formula contains six variable parameters. Table 4 lists the optimized parameter values for the NO_x and the PM formula. The parameters for the NO_x model diverge moderately for the two data sets. In contrast, the PM model parameters are much different for the two data sets.

The resulting small number of parameters of the models guarantees their fast application to other engine types. In contrast to the ANN model used for the IVS algorithm, the number of parameters needed can be reduced by a factor of 10. In addition, the reduced number of parameters is directly correlated with the amount of measurement data needed for the calibration of the model. Figure 10 shows the calibration of the model on the heavy-duty engine data set for different training data fractions. The whole data set contains 258 measurement data points. Fifty randomly chosen measurement data points are adequate to calibrate the model parameters as the performance on the validation data set is comparable to the performance on the test data set. Therefore, the number of measurement data to calibrate the models can be reduced significantly.

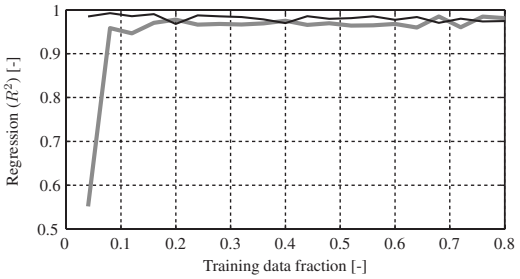

Fig. 10 Regression performance of the NO_x emissions for the heavy-duty engine data set for different training data fractions: training data set (black) and validation data set (gray)

6 Estimating the Selected Relevant Engine Process Variables During Transients

Some of the transient inputs into the set point deviation model can be provided directly by standard sensor signals of the ECU. Nevertheless, several additional parts of the engine must be modeled to estimate all of the selected relevant engine process variables. If the REM is used as a virtual sensor, the cylinder charge variables (m_e, x_{air}) and the combustion characteristics ($\varphi_{B50}, \varphi_{B90}$) must be estimated by a model. Figure 11 shows the signal flow chart of the three combined models. The EGR mass flow is not measured during transient operation of the test bench due to the slow dynamics of the available CO_2 measurement device. Therefore, the cylinder charge estimation is necessary to compare the REM estimations with measurement data. The combustion characteristics are measurable with a real-time cylinder pressure evaluation available at the test bench. The combustion model is optional in this case. The cylinder charge variables are estimated by a simple gas path model discussed in Sec. 6.1. The combustion model is presented in Sec. 6.2.

If the emission model is used as a standalone, the entire engine systems must be modeled. This includes the intake air path, the exhaust gas path, the turbocharger, the EGR system, the gas-exchange cycle, and the combustion cycle. In this case, all the necessary dynamic signals can be estimated by a state-of-the-art mean-value engine model [23].

6.1 Cylinder Charge Estimation. The cylinder charge (mass and gas composition) at intake valve closing must be estimated by a model due to the lack of an EGR mass flow sensor. The remaining gas path signals are measured directly by standard ECU sensors. The EGR mass flow estimation is based on the intake mass flow sensor signal and an engine mass flow estimation. The mass flowthrough into the engine can be estimated as follows:

Table 4 Parameter values of the resulting formulas

	C_1	C_2	C_3	C_4	C_5	C_6	C_7	C_8
Light-duty engine								
NO_x	⋯	8.36	⋯	−8.94	−4.54	⋯	−2.41	−2.58
PM	5.01	−775	152	−45.4	⋯	2.86	−1.33	⋯
Heavy-duty engine								
NO_x	⋯	−3.61	⋯	3.03	−3.17	⋯	−3.04	−4.06
PM	1.73	−0.02	463	−1.99	⋯	0.06	0.31	⋯

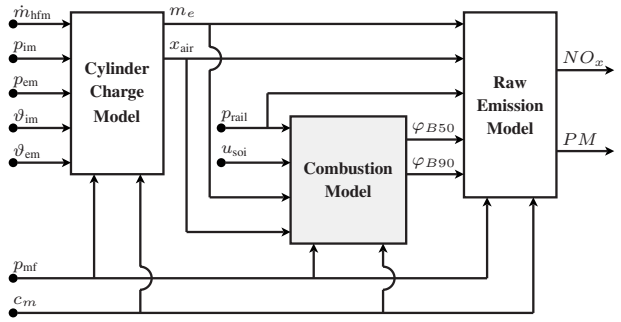

Fig. 11 Interactions of the three models: virtual sensor application

$$\dot{m}_{e,\text{in}} = \lambda_l(c_m, p_{\text{mf}}) \frac{V_d \omega_e \rho_{\text{im}}}{4\pi} \tag{19}$$

where $\lambda_l(c_m, p_{\text{mf}})$ is the volumetric efficiency and ρ_{im} is the density of the air in the intake manifold. The volumetric efficiency is mainly a function of the mean piston speed and the fuel mean pressure. The EGR mass flow can now be calculated as

$$\dot{m}_{\text{egr}} = \frac{d}{dt} m_{\text{im}} + \dot{m}_{e,\text{in}} - \dot{m}_{\text{hfm}} \tag{20}$$

where $\dot{m}_{\text{hfm}}$ is the intake air mass flow sensor signal and m_{im} is the mass in the intake manifold. The mass in the intake manifold is calculated using the ideal gas law. If the temperature in the intake manifold ϑ_{im} is assumed to be slowly varying, the derivative of the mass is estimated as

$$\frac{d}{dt} m_{\text{im}} = \frac{d}{dt} p_{\text{im}} \frac{V_{\text{im}}}{R \cdot \vartheta_{\text{im}}} \tag{21}$$

where $(d/dt)p_{\text{im}}$ is the derivative of the intake manifold pressure signal, V_{im} is the manifold volume, and R is the gas constant. The internal residual gas mass is estimated as follows:

$$m_{\text{rg}} = \frac{p_{\text{em}} V_c}{R \vartheta_{\text{em}}} \tag{22}$$

where p_{em} is the exhaust manifold pressure, ϑ_{em} is the engine-out temperature, V_c is the top dead center cylinder volume, and R is the gas constant of the exhaust gas.

The following sensor signals must be available to estimate the cylinder charge:

- intake mass flow sensor
- pressure sensor in the intake manifold
- pressure sensor in the exhaust manifold
- temperature sensor in the intake manifold
- temperature sensor in the exhaust manifold
- engine speed

If no exhaust manifold pressure sensor is available, the signals must be estimated by a model, or the internal EGR mass must be calculated by a different approach.

6.2 Combustion Model. In addition, a combustion model is generated using the same methodology as for the REM. The combustion model estimates the combustion center and the location of the 90% fuel mass burnt. This model is necessary if no cylinder pressure sensor signal is available. The structure of the combustion model is similar to the emission model. Again, the model is formulated as an extended quasistationary approach. The combustion center is calculated as follows:

$$\varphi_{B50} = u_{\text{soi}} + \Delta\varphi_{B50} \tag{23}$$

where u_{soi} is the start of injection angle and $\Delta\varphi_{B50}$ is the duration between start of injection and location of 50% fuel mass burnt

Table 5 Technical data of the test bench engines

Type	HD DI	LD DI
Feature	EGR, twin scroll turbine	EGR, VNT
Displacement	6.51	3.01
Cylinders	6	6

expressed in crank angle degrees. Then, $\Delta\varphi_{B50}$ is estimated as

$$\Delta\varphi_{B50} = \gamma_{\Delta\varphi_{B50}} \Delta\varphi_{B50_0} \tag{24}$$

where $\Delta\varphi_{B50_0}$ is the mapped quasistationary value and $\gamma_{\Delta\varphi_{B50}}$ is the correction factor. The correction factor is a function of the operating point, the cylinder mass m_e, the air fraction at the closed intake valve x_{air}, and the fuel rail pressure p_{rail},

$$\gamma_{\Delta\varphi_{B50}} = f(c_m, p_{\text{mf}}, \gamma_{m_e}, \gamma_{x_{\text{air}}}, \gamma_{p_{\text{rail}}}) \tag{25}$$

The functional coherences are derived again by the symbolic regression algorithm. The location of 90% fuel mass burnt is estimated similarly as

$$\varphi_{B90} = u_{\text{soi}} + \Delta\varphi_{B90} \tag{26}$$

Then, $\Delta\varphi_{B90}$ is calculated as

$$\Delta\varphi_{B90} = \gamma_{\Delta\varphi_{B90}} \Delta\varphi_{B90_0} \tag{27}$$

where the correction factor $\gamma_{\Delta\varphi_{B90}}$ is estimated as

$$\gamma_{\Delta\varphi_{B90}} = f(c_m, p_{\text{mf}}, \gamma_{m_e}, \gamma_{x_{\text{air}}}, \gamma_{p_{\text{rail}}}, \gamma_{u_{\text{soi}}}) \tag{28}$$

If necessary, other combustion variables such as peak pressure, maximum heat release rate, or location of 10% fuel mass burnt can be estimated analogously. The following ECU signals must be provided to estimate the combustion characteristic variables:

- start of injection
- fuel rail pressure
- injected fuel mass
- engine speed

The other required signals (m_e, x_{air}) are estimated by the cylinder charge model.

7 Experimental Setup

The measurements are carried out on the two different engine types shown in Table 5. Both are modern common-rail DI diesel engines equipped with a turbocharger and a high-pressure EGR system. A base map of both engines is measured. In addition, all the actuator inputs are varied in six relevant operating points, well distributed over the engine operating range. The systematic variations are measured starting from the base map settings. Single and double actuator variations are conducted to cover the entire operating range of the engine. The data sets of both engines include approximately 300 static measurement points. Measurements of dynamic operation are conducted as well to test the transient prediction capability of the proposed control-oriented emission model. The measurements include load steps at constant engine speed, accelerations at constant load, and transient engine cycles like the European transient cycle (ETC).

The exhaust emissions are measured with an AVL CEB II gas analyzer. The PM emissions are measured with an AVL 430 opacimeter and an AVL 415 S smoke meter. During the transient measurements, a fast nitric oxide (NO) sensor is used (Cambustion CLD 400). A correlation curve is used to calculate the filter smoke number based on the opacity signal during the transient operation. The EGR rate is estimated based on CO_2 measurements in the intake and the exhaust manifolds. All the signals are stored at 100 Hz. The ECU signals are delivered to the recorder by the CAN bus. During transient measurements, the ECU variables are also

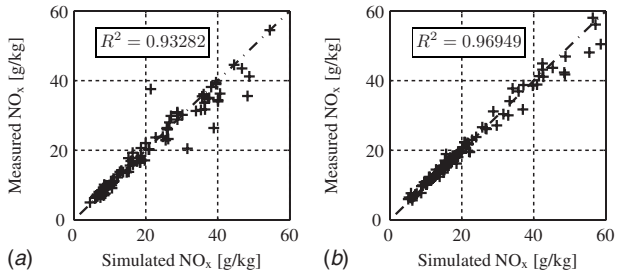

Fig. 12 Regression plot of the NO_x emissions: (*a*) LD and (*b*) HD engine types using in-cylinder pressure sensors

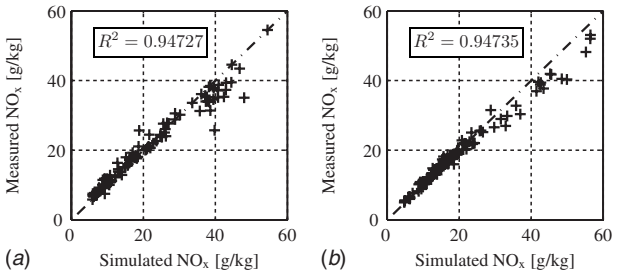

Fig. 14 Regression plot of the NO_x emission model coupled with the combustion model: (*a*) LD and (*b*) HD engine types without using in-cylinder pressure sensors

stored on the ECU application computer, at 1 kHz or 200 Hz, respectively. The measurement data are synchronized by reference signals stored on both recorders.

8 Results and Discussion

The simulation results of the model structures derived with the proposed method show a good correlation with the static measurement data. Figures 12 and 13 show the results of the NO_x and PM emission model for the light-duty (LD) and the heavy-duty (HD) engine types for the total data sets including the training and the validation data. The regression of the PM emission is worse due to the relatively high measurement errors, especially for low filter smoke numbers. Overall, the model performs better on the HD engine data set. This fact can be explained by the two different base maps used for the LD engine measurements. Unfortunately, for the LD engine only static and dynamic measurement data with different base maps were available. The transient measurements are carried out with a different start of injection timing. Therefore, the base map used for the transient measurements is taken to calculate the correction factor values for the static measurement data as well. Hence, large correction factors occur in most static measured actuator variations. The results are comparable with those obtained from the neural network approach used in the IVS algorithm, even though the number of parameters is reduced by a factor of 10. The portability of the emission models is shown with the two data sets used from engines of very different sizes. This corroborates the use of well selected characteristic engine process variables as inputs to the nonlinear statistical model. Figures 14 and 15 show the results of the NO_x and PM emission model coupled with the combustion model for the light-duty and the heavy-duty engine types. The performance of the total model is comparable to the results of the emission model only. Therefore, the estimation of the combustion center and combustion end can be used instead of cylinder pressure sensor data. Figure 16 shows the results of the emission model using nonoptimized parameters. The parameters of the LD engine data set are used to calculate the emissions of the HD engine data set. The performance obtained with the nonoptimized parameters shows the portability not only of the derived structure but also of the parameters even though the estimation of the PM emissions has some outliers.

The extended quasistationary model trained on static measurement data is then tested with the same parameters during transient operating conditions to show its extrapolation capabilities. All the transient results shown are measurement data from the light-duty engine. The transient simulations are conducted together with the cylinder charge and the combustion model to estimate the mass composition when the intake valve is closed and the combustion characteristics, respectively. Figure 17 shows a comparison between measurement data and simulation results of the combustion model during a load step. Due to the smaller amount of air mass in the cylinder, the combustion process takes longer during the transient phase. Figure 18 shows the performance of the REM during a load step from 20% to 80%. The results of the simulation agree well with the measurement data. During the turbolag phase, the amount of PM emissions detected is ten times higher. Nevertheless, the emission model is able to predict these high deviations. In this phase, the NO_x emissions are lower than those in static operation due to the reduced amount of oxygen available during combustion. The transient characteristics of the investigated engine are simular to results reported in Ref. [24]. The oscillation of the NO_x emission observable after the load step is due to the

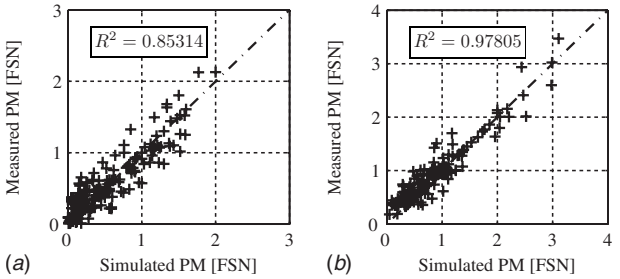

Fig. 15 Regression plot of the PM emission model coupled with the combustion model: (*a*) LD and (*b*) HD engine types without using in-cylinder pressure sensors

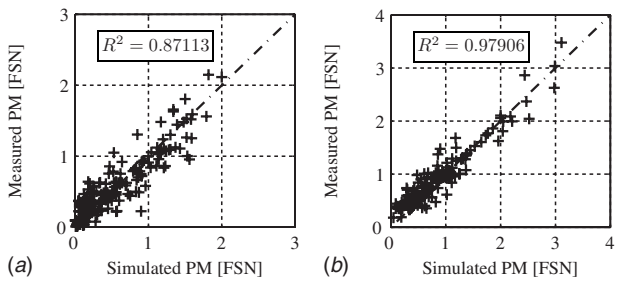

Fig. 13 Regression plot of the PM emissions: (*a*) LD and (*b*) HD engines using in-cylinder pressure sensors

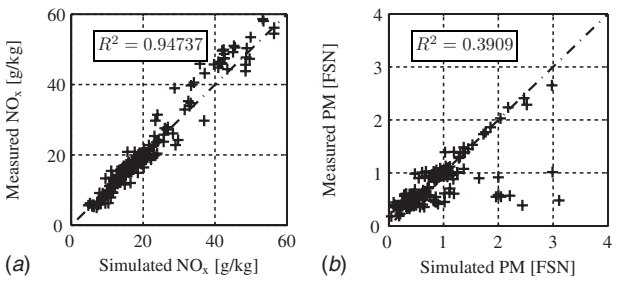

Fig. 16 Regression plot of the emission model using the HD engine data set with the LD engine parametrization, NO_x: (*a*) PM and (*b*) emissions

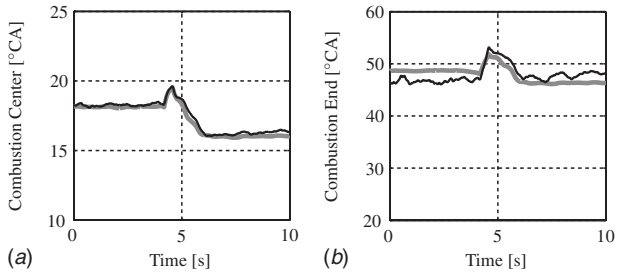

Fig. 17 Comparison of measurement data and simulation results of the combustion model during a load step from 20% to 80% at 2250 rpm: measurement (black) and combustion model (gray)

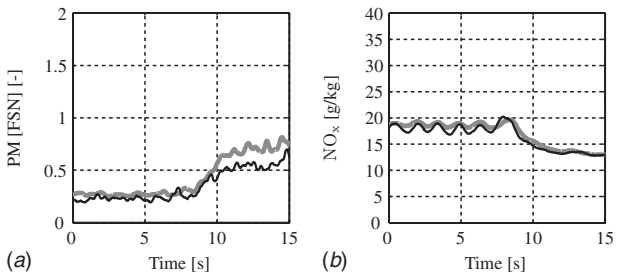

Fig. 20 Comparison of simulation results and measurement data of (*a*) PM and (*b*) NO_x emissions during a boost pressure step from 2.1 bars to 1.7 bars: measurement (black) and raw emission model (gray)

oscillating EGR valve. Since the control of the engine was still under development, the transient behavior of the EGR controller is not optimized yet, which explains these oscillations. However, the model is able to predict this oscillation for both species of engine-out emissions.

Figures 19–22 show simulation results of actuator steps. The actuator steps are carried out at 60% load and an engine speed of 2000 rpm. The gas path actuators (EGR valve and turbine actuator) influence the boundary condition of the combustion dynamically. The slow increase in boost pressure due to the turbo lag is evident in the emission data as well. The PM emissions are more sensitive to lower boost pressure than the NO_x emissions. In contrast, the higher EGR rate reduces the NO_x emissions by one-half. The mixing dynamics of the intake receiver and the EGR controller significantly influence the EGR mass at the closed intake valve. In contrast, the very fast injection actuators also cause a step in the emissions. The only relevant dynamics are the exhaust path delay time and the gas mixing process in the exhaust system.

9 Conclusion

The purpose of this analysis was to formulate a method to derive a control-oriented model of the raw emissions of a diesel engine. The mixed physics and regression approach proposed simplifies the generation of nonlinear models. In addition, the models derived are advantageous due to their increased portability to other engines. The methodology proposed in this paper is applicable to various modeling problems.

The method drastically reduces the calibration effort due to the reduced number of parameters needed to describe the transient raw emissions. The model is formulated using an extended quasistationary approach. The extension to the base map part describes the set point deviations during transient operating conditions of the engine. The deviations are predicted using correction factors. Due to the extended quasistationary approach, the raw emission model can be calibrated with static measurement data, which lowers the application costs of the model and the requirements for the test bench.

The inputs to the raw emission model are chosen by an input variable selection procedure based on a genetic-programming

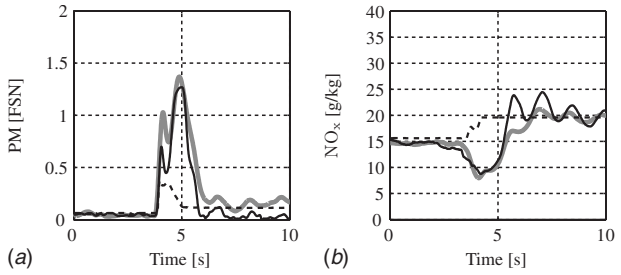

Fig. 18 Comparison of simulation results and measurement data of (*a*) PM and (*b*) NO_x emissions during a load step from 20% to 80% at 2000 rpm: measurement (black), raw emission model (gray), and base map value (dashed)

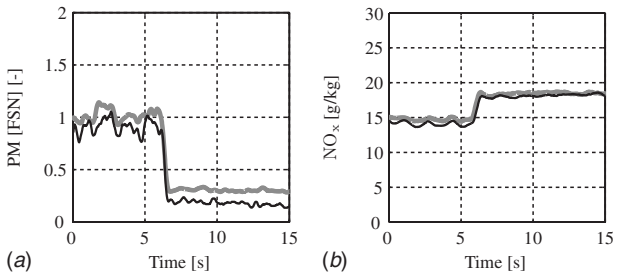

Fig. 21 Comparison of simulation results and measurement data of (*a*) PM and (*b*) NO_x emissions during a fuel rail pressure step from 600 bars to 800 bars: measurement (black) and raw emission model (gray)

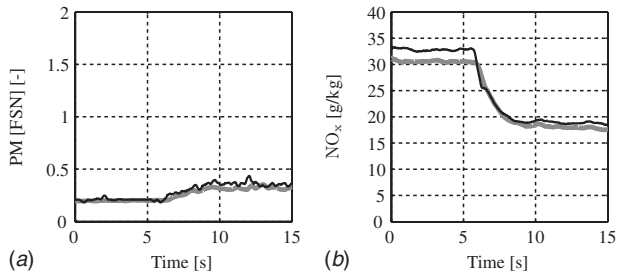

Fig. 19 Comparison of simulation results and measurement data of (*a*) PM and (*b*) NO_x emissions during an EGR-rate step from 0% to 10%: measurement (black) and raw emission model (gray)

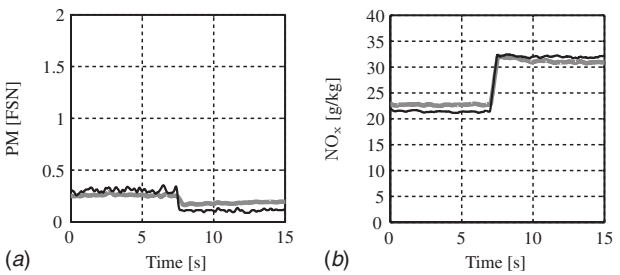

Fig. 22 Comparison of simulation results and measurement data of (*a*) PM and (*b*) NO_x emissions during the start of injection in crank angle (CA) before top dead center (bTDC): measurement (black) and raw emission model (gray)

wrapper approach. The input selector is fed with some 40 characteristic process variables. Due to the highly redundant process variables used as candidates, the input variable selection algorithm proposes a selection of promising subsets. As expected, several combinations show a comparable performance. The practitioner has the option of choosing a subset of inputs that is easy to measure or to estimate.

The functional structure of the raw emission model is derived with a symbolic regression algorithm. The toolbox used is extended with a local search algorithm to calibrate the parameters of the functional relations generated. The separation of the input variable selection task from the model structure generation significantly reduces the computational effort. The performance of the derived model is similar to that of an ANN with around ten times more parameters. The method used is tested on two different engine types, and it yields similar results.

The raw emission model is embedded in a simple gas path mean value and in a combustion model. The combination of the three models allows an estimation of the raw emissions in transient operating conditions, for example, as virtual sensor directly in the ECU. The extended quasistationary approach is able to predict the quantities of the raw emissions during various transients. Hence, the extrapolation capability of the control-oriented model is shown.

Acknowledgment

The authors gratefully acknowledge the financial support by the European Union in the Integrated Project European Commission FP6 Program. The current investigation was conducted during the integrated project "GREEN" (Grant No. TIP4-CT-2005-516195). Also, the authors would like to express our gratitude to the subproject coordinator Daimler AG and the subproject partner AVL List GmbH for providing the experimental data.

References

[1] Guzzella, L., and Amstutz, A., 1998, "Control of Diesel Engines," IEEE Control Syst. Mag., **18**(5), pp. 53–71.
[2] Ammann, M., Fekete, N., Amstutz, A., and Guzzella, L., 2001, "Control-Oriented Modelling of a Turbo-Charged Common-Rail Diesel Engine," Conference on Control and Diagnostics on Automotive Applications, Sestri Levante, Italy.
[3] Ericson, C., and Westerberg, B., 2005, "Transient Emission Prediction With Quasi Stationary Models," SAE Technical Paper No. 2005-01-3852.
[4] Christen, U., and Vantine, K., 2001, "Event-Based Mean-Value Modeling of DI Diesel Engines for Controller Design," SAE Technical Paper No. 2001-01-1242.
[5] Arsie, I., Pianese, C., and Rizzo, G., 1998, "Enhancement of Control Oriented Engine Models Using Neural Network," *Proceedings of the Sixth IEEE Mediterranean Conference on "Control System*," Alghero, Italy.
[6] Hiroyasu, H., 1985, "Diesel Engine Combustion and Its Modeling," *Proceedings of COMODIA Symposium on Diagnostics and Modeling of Combustion in Reciprocating Engines*, Tokyo, Japan, pp. 53–75.
[7] Amsden, A., Ramshaw, J., O'Rourke, P., and Dukowicz, J., 1985, "Kiva: A Computer Program for Two- and Three-Dimensional Fluid Flows With Chemical Reactions and Fuel Sprays," Los Alamos National Laboratory, Technical Report No. LA-10245-MS.
[8] Gärtner, U., 2001, "Die Simulation der Stickoxid Bildung in Nutzfahrzeug-Dieselmotoren," Ph.D. thesis, University of Darmstadt.
[9] Traver, M., and Atkinson, R., 1999, "Neural Network-Based Diesel Engine Emissions Prediction Using In-Cylinder Combustion Pressure," SAE Technical Paper No. 1999-01-1532.
[10] del Re, L., and Langthaler, P., 2005, "NO_x Virtual Sensor Based on Structure Identification and Global Optimization," SAE Technical Paper No. 2005-01-0050.
[11] Rakopoulos, C., Giakoumis, E., and Rakopoulos, D., 2004, "Cylinder Wall Temperature Effects on the Transient Performance of a Turbocharged Diesel Engine," Energy Convers. Manage., **45**, pp. 2627–2638.
[12] Schilling, A., Amstutz, A., Onder, C. H., and Guzzella, L., 2006, "A Real-Time Model for the Prediction of the NO_x Emissions in DI Diesel Engines," *Proceedings of the 2006 IEEE International Conference on Control Applications*, Munich, Germany, pp. 2042–2047.
[13] Kohavi, R., and John, G. H., 1997, "Wrappers for Feature Subset Selection," Artif. Intell., **97**(1–2), pp. 273–324.
[14] Koza, J., 1992, *Genetic Programming: On the Programming of Computers by Means of Natural Selection*, MIT, Cambridge, MA.
[15] Siebers, D., 1999, "Scaling Liquid-Phase Fuel Penetration in Diesel Sprays Based on Mixing-Limited Vaporization," SAE Technical Paper No. 1999-01-0528.
[16] Bayer, J., and Foster, D., 2003, "Zero-Dimensional Soot Modeling," SAE Technical Paper No. 2003-01-1070.
[17] Jang, J.-S., 1996, "Input Selection for ANFIS Learning," *Proceedings of the Fifth IEEE International Conference on Fuzzy Systems*, New Orleans, Vol. 2, pp. 1493–1499.
[18] May, R. J., Maier, H. R., Dandy, G. C., and Fernando, T. G., 2008, "Non-Linear Variable Selection for Artificial Neural Networks Using Partial Mutual Information," Environ. Modell. Software, **23**(10–11), pp. 1312–1326.
[19] Joliffe, I. T., 1986, *Principal Component Analysis*, Springer-Verlag, New York.
[20] Maertens, K., Babuska, R., and De Baerdemaeker, J., 2005, "Evolutionary Input Selection for the Non-Linear Identification of Complex Processes," Comput. Electron. Agric., **49**(3), pp. 441–451.
[21] Silva, S., 2007, GPLAB: A Genetic Programming Toolbox for MATLAB, ECOS–Evolutionary and Complex Systems Group, University of Coimbra.
[22] Lagarias, J. C., Reeds, J. A., Wright, M. H., and Wright, P. E., 1998, "Convergence Properties of the Nelder-Mead Simplex Method in Low Dimensions," SIAM J. Optim., **9**(1), pp. 112–147.
[23] Guzzella, L., and Onder, C. H., 2004, *Introduction to Modeling and Control of Internal Combustion Engine Systems*, Springer-Verlag, New York.
[24] Hagena, J., Filipi, Z. S., and Assanis, D., 2006, "Transient Diesel Emissions: Analysis of Engine Operation During a Tip-in," SAE Technical Paper No. 2006-01-1151.